THE JOURNAL OF PHYSICAL CHEMISTRY LETTERS
A JOURNAL OF THE AMERICAN CHEMICAL SOCIETY

pubs.acs.org/JPCL

Letter

Magnetic Gap of Fe-Doped $BiSbTe_2Se$ Bulk Single Crystals Detected by Tunneling Spectroscopy and Gate-Controlled Transports

Rikizo Yano,*,+ Andrei Kudriashov, Hishiro T. Hirose, Taiki Tsuda, Hiromi Kashiwaya, Takao Sasagawa, Alexander A. Golubov, Vasily S. Stolyarov,*,+ and Satoshi Kashiwaya*

Cite This: J. Phys. Chem. Lett. 2021, 12, 4180–4186

Read Online

ACCESS | Metrics & More | Article Recommendations | Supporting Information

ABSTRACT: Topological insulators with broken time-reversal symmetry and the Fermi level within the magnetic gap at the Dirac cone provides exotic topological magneto-electronic phenomena. Here, we introduce an improved magnetically doped topological insulator, Fe-doped $BiSbTe_2Se$ (Fe-BSTS) bulk single crystal, with an ideal Fermi level. Scanning tunneling microscopy and spectroscopy (STM/STS) measurements revealed that the surface state possesses a Dirac cone with the Dirac point just below the Fermi level by 12 meV. The normalized dI/dV spectra suggest a gap opening with Δ_{mag} ~55 meV, resulting in the Fermi level within the opened gap. Ionic-liquid gated-transport measurements also support the Dirac point just below the Fermi level and the presence of the magnetic gap. The chemical potential of the surface state can be fully tuned by ionic-liquid gating, and thus the Fe-doped BSTS provides an ideal platform to investigate exotic quantum topological phenomena.

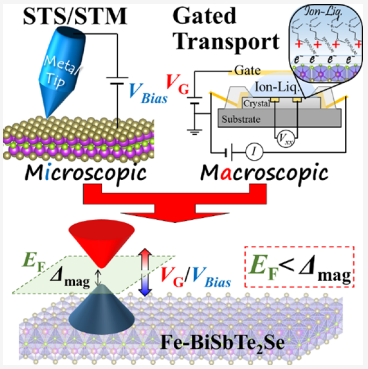

Topological insulators (TIs) possess a unique time-reversal invariant surface (edge) state, the so-called massless Dirac cone (e.g., linear band dispersion), which offers high-mobility carriers and promising spin functionalities.[1−10] Breaking time-reversal symmetry on TIs by applying a large magnetic field or magnetization annihilates the time-reversal invariant point (the Dirac point: DP) and opens the magnetic gap, Δ_{mag} (the so-called massive Dirac cone). The massive Dirac state induces remarkable topological phenomena, such as the quantum anomalous Hall (QAH) effect and the image magnetic monopole. Besides, fabricating heterostructures with other magnetic insulators or superconductors, the chiral edge states produce topological electromagnetic (ME) effects and virtual exotic elementary particle states, e.g., axion ME terms and Majorana Fermions.[2,11−13]

There are two key factors in the observation of the surface-driven phenomena: ideal Fermi level E_F (within the magnetic gap and the bulk bandgap) and high bulk insulating nature. For nonmagnetic TIs, tremendous efforts have been put into alloying appropriate Bi−Sb−Te−Se compositions considering defect chemistry[14−18] to overcome the two drawbacks. On the other hand, achieving high bulk insulating magnetic TI is still challenging. The common approach is to utilize a thin film of magnetic TIs to reduce the bulk conduction contribution.[19−23] While Cr-doped $(Bi, Sb)_2Se_3$[19] and $MnBi_2Te_4$[24] thin films exhibit the QAH effect, bulk magnetic TIs will provide complicated heterostructure devices with a high degree of freedom.

In the context of searching for desirable bulk materials, we focus on Fe as a dopant into (Bi,Sb) sites in Bi based tetradymites. The tetradymites have layered crystal structures (Figure 1a). We should care about the unintended intergrowth of magnetic impurities of Fe−Se compounds promoted by Fe doping.[25−27] This intergrowth may occur over a certain temperature range and be easily driven by an inhomogeneous Fe distribution. Indeed, owing to special care such as homogeneous mixing at high temperatures and rapid quenching, we grew Fe-doped Bi_2Te_2Se and Fe-doped $BiSbTe_2Se$ (Fe-BSTS) as high bulk-insulating magnetically doped TIs[28,29] and reported observation of unusual proximity effects.[28] However, the detailed electronic structure, in particular, the location of the DP and E_F, is still an open question.

Here, we report the detailed electronic band structure of the Fe-BSTS. Its schematic band structures above and below the Curie temperature (T_{Curi}) are summarized in Figure 1b,c, respectively. We performed *in situ* cleavage scanning tunneling microscopy and spectroscopy (STM/STS) measurements. Fe-BSTS has a high bulk insulating nature with a bandgap of Δ_{bulk} ~400 meV, and the Fermi level E_F is found to be close to the DP (E_{DP}). Furthermore, we discovered a magnetic gap Δ_{mag} at the DP. The transport measurements tuned with electric-double-layer transistors (EDLTs) also support these surface

Received: March 17, 2021
Accepted: April 12, 2021
Published: April 26, 2021

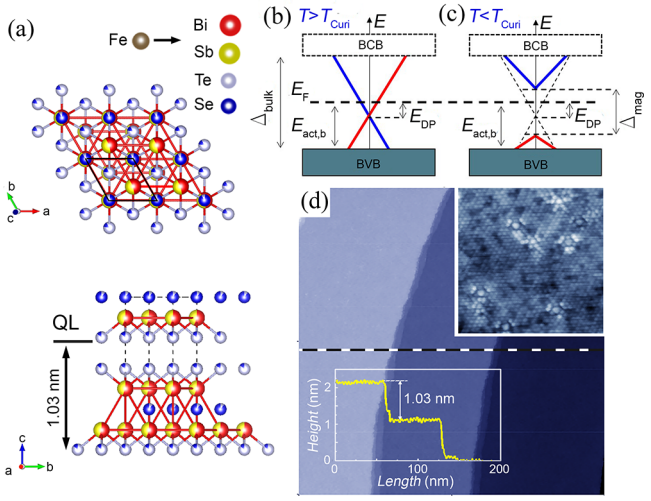

Figure 1. Summarized band structures and scanning tunneling microscopy. (a) The crystal structure of Fe-BSTS. The upper and bottom figures indicate the top view and the layered structure, respectively. The arrow indicates a single quintuple layer (QL). Band structures of Fe-BSTS (b) above and (c) below the Curie temperature. The parameters were determined by STM and gate-tuned transports. Δ_{mag}= 55 meV, E_{DP} = −12 meV, and $E_{act,b}$ = 33.3 meV (see text for more details). (d) A 200 nm × 200 nm STM image (bias voltage V_T = 183 mV and tunnel current I_T = 104 pA) of the *in situ* cleaved crystal. Atomically flat terraces are separated by 1.03 nm height steps (the bottom left inset depicts the profile along the dashed line of the STM image), and the height of the terraces corresponds to QL. In the top-right inset, a 10 nm × 10 nm atomically resolved image with a typical set of defects.

states. Combining microscopic STS and macroscopic transport results consistently ensures an ideal E_F position within Δ_{mag} at a very low temperature.

Owing to the excellent cleavage property of Fe-BSTS, sizable crystals were cleaved in the chamber, and an atomically flat surface enabling STM/STS measurements was obtained. STM mapping with a constant current of 104 pA and a bias voltage of 183 mV (Figure 1d) show clear atomically flat terraces. The observed step height was 1.03 nm (Figure 1d, inset), which corresponds to a five atomic layer, the so-called quintuple layer (QL) of Fe-BSTS, as shown in Figure 1a. These QLs are weakly bonded by van der Waals forces and terminated by chalcogen atoms (Se, Te). A local STM study of the flat terraces revealed well-ordered hexagonal lattices with randomly arranged atomic defects, reflecting its homogeneous substitution of (Bi, Sb, Fe) and (Te, Se) sites (see Figure 1a, the inset). We confirmed that the spatial electron density distribution near defects (not shown here) showed a typical spectrum for other Bi based tetradymites.[30−32] The form of fingerprints depends on the type of defects and their depth in the QLs;[33] e.g., the surface has bright triangular dots corresponding to the chalcogen vacancies described in ref 34.

Figure 2a shows the averaged STS spectra measured at 4.2 K (blue line) and 77 K (red). The rapid rise around V_T = −100 mV and 300 mV corresponds to the bulk valence band (BVB) and bulk conduction band (BCB), respectively, and thus the bulk bandgap is Δ_{bulk} ≃400 meV (marked as a green-white gradient). The zero-bias voltage (Fermi energy E_F) is located close to the BVB, a hallmark of a p-type semiconductor. Within the bandgap, almost linear spectra appeared regardless of the measurement spots (see the inset of Figure 2a), which is a topologically protected feature, and the linear band represents the surface states (the Dirac cone). The DP was estimated as E_{DP} ∼−12 meV from the extrapolation of the linear part of the spectra (inset of Figure 2a). Furthermore, the normalized spectrum of dI/dV (4.2 K) divided by the dI/dV (77 K)[35] reveals some gaps around the DP (see Figure 2b). Based on previous reports (T_{Curri} < 50 K)[28,36] and other magnetically doped tetradymite systems (T_{Curri} ∼10 K),[22,23] the measurement temperatures should cross the Curie temperature of the present material, and the observed gap represents the magnetic gap at the DP with a size of Δ_{mag} ∼55 meV, which is comparable to other magnetic TIs.[36−38] We link the fact that the magnetic gap is partially filled in the region of the Dirac point because of the temperature fluctuations and the large number of atomic defects saturating the magnetic gap by electrons giving a nonzero background. The gap at the time-conserved DP is a hallmark of the broken time-reversal symmetry due to ferromagnetic ordering, whereas typical other origins, e.g., the Kondo effect,[39] produce the gap structure at the E_F.

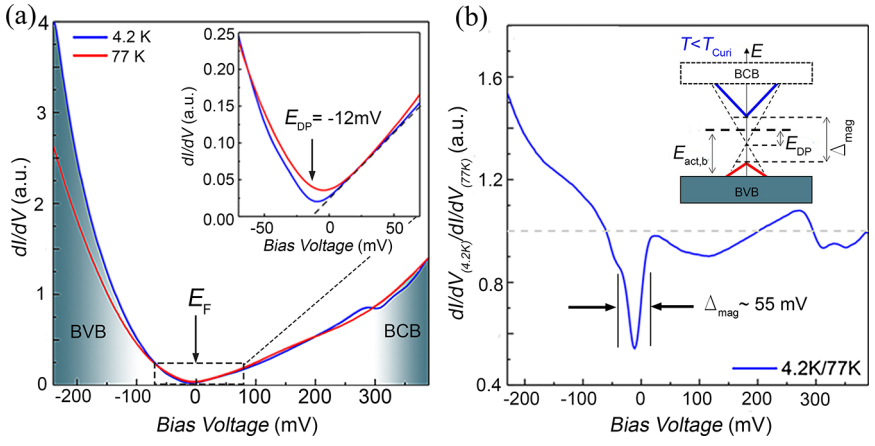

Figure 2. Scanning tunnelling spectroscopy. (a) Average tunnelling spectra at 4.2 K (blue line) and 77 K (red line). The inset shows a highlight around the zero-bias voltage. The dashed line represents a linear dispersion approximation, and the arrow indicates the estimated Dirac point at −12 mV. (b) Normalized dI/dV spectrum of 4.2 K by the 77 K spectra. A clear 55 mV gap appears near the Dirac point. Insets are schematic surface structures below the Curie temperature.

https://doi.org/10.1021/acs.jpclett.1c00869
J. Phys. Chem. Lett. 2021, 12, 4180−4186

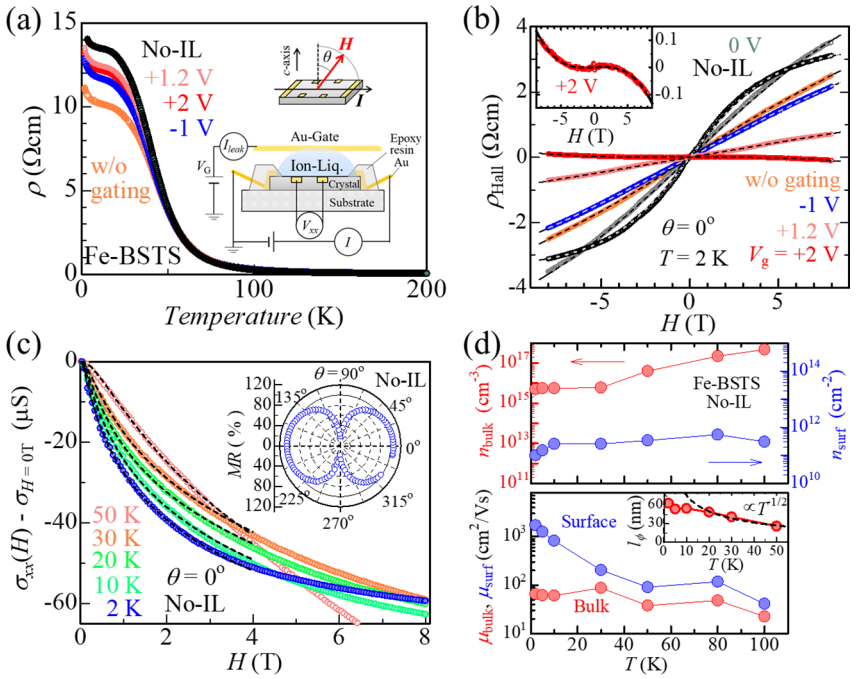

Figure 3. Experimental setups and transport properties of a Fe-BSTS. (a) Temperature dependence of resistivity with and without gating voltage. The label "w/o gating" indicates the measurement performed just after loading the ionic-liquid (IL) but without applying external gating voltage. The inset is the schematic of a transport measurement setup with IL gating on a bulk single crystal. (b) Hall resistivity for various gating voltages at 2 K. The inset shows a zoomed-in plot for V_G = +2 V. Dashed lines for each plot represent the best fitting results by the two-band model. (c) Change in sheet magnetoconductance of No-IL (without IL) with a perpendicular magnetic field at several temperatures ranging from 2 to 50 K. The dashed black lines represent fitting results at 2−30 K by the HLN model. The inset shows a polar plot of the magnetoresistance of the No-IL crystal with a magnetic field of 8 T at 2 K. (d) Temperature dependences of the carrier (top panel) and mobility (bottom panel) for the bulk and surface of the as-grown Fe-BSTS crystal (No-IL). The inset is the temperature dependence of the phase coherence length obtained using the HLN model. The dashed line is a fitting result for $T^{-1/2}$ above 20 K.

The inset of Figure 2b shows the schematic band structure determined from the STS dI/dV spectra. The most prominent feature is that the location of the Fermi level is just above the DP and within the magnetic gap, which is an ideal situation to observe exotic magnetic gap-origin phenomena described in the introduction section.

We investigated the transport properties of the gate-controlled Fe-BSTS bulk single crystal to determine the locations of the E_F and the E_{DP}. The ionic-liquid (IL) gating in EDLT enables effective carrier control just near the surface (typical effective depth ∼several nanometers).[40−43] In general, this technique is applied to thin-film materials nowadays, and it is difficult to achieve ambipolar conduction for bulk materials.[44] In contrast, we observed the ambipolar surface carrier conduction of Fe-BSTS even using a bulk crystal, owing to its high surface mobility. The experimental setup is shown in the inset of Figure 3a. Further details are provided in the Supporting Information. Because loading the IL itself affects carrier density, we labeled "No-IL" and "w/o gating" as the state of the as-grown crystal without IL and just after loading IL but without voltage-control, respectively. The positive gate voltage provides electron carrier doping at the top of the crystal. All gate-voltage controlling took place after cooling to 230 K in a vacuumed chamber to prevent chemical reactions.

As a first step, we evaluated the as-grown Fe-BSTS bulk crystal (No-IL). The temperature dependence of resistivity showed insulating above 50 K, whereas the slope decreased below 25 K, as shown in Figure 3a. Interestingly, the resistivity increased again below 10 K and did not follow the typical −log T dependence expected for the Kondo effect which is often observed in nonmagnetic TIs, e.g., in refs 45 and 46. The magnetotransport properties also change around this temperature, as discussed later in the transport section. Therefore, we claim this upturn can be ascribed to the gap opening near 10 K. The high-temperature resistivity followed three-dimensional variable range hopping, which is commonly observed in TIs with highly insulation in the bulk.[14,17,45,47] From the standard Arrhenius plot, the value of the activation energy for the bulk was determined to $E_{act,b}$ = 33.3 meV. Referring to Figure 1b,c, the values of E_{DP}, Δ_{mag}, and $E_{act,b}$ are consistent with the estimated band structure, i.e., the Fermi level should be located within the magnetic gap at low temperatures.

The dominant surface contribution was confirmed from magnetoresistance (MR = $(\rho(H) - \rho(0))/\rho(0)$), magnetoconductance, and Hall resistivity (Figure 3b). Detailed MR data are summarized in the Supporting Information. The 2-fold rotational symmetry in the MR is a characteristic of the two-dimensional electron nature from the surface states (inset of Figure 3c). Figure 3c shows the sheet magnetoconductance and fitting results (black lines) using the simple Hikami−Larkin−Nagaoka (HLN) model[46,48] for weak antilocalization (WAL):

$$G(B) - G(0) \simeq \alpha \frac{e^2}{2\pi^2\hbar}\left[\Psi\left(\frac{1}{2} + \frac{B}{B_\phi}\right) - \ln\left(\frac{B}{B_\phi}\right)\right]$$

where α, e, $\hbar$, and Ψ are the WAL coefficient, electronic charge, reduced Planck constant, and digamma function, respectively. The $\alpha \sim -1$ was obtained at the low-temperature region. From the characteristic magnetic field, B_ϕ, the

https://doi.org/10.1021/acs.jpclett.1c00869
J. Phys. Chem. Lett. 2021, 12, 4180−4186

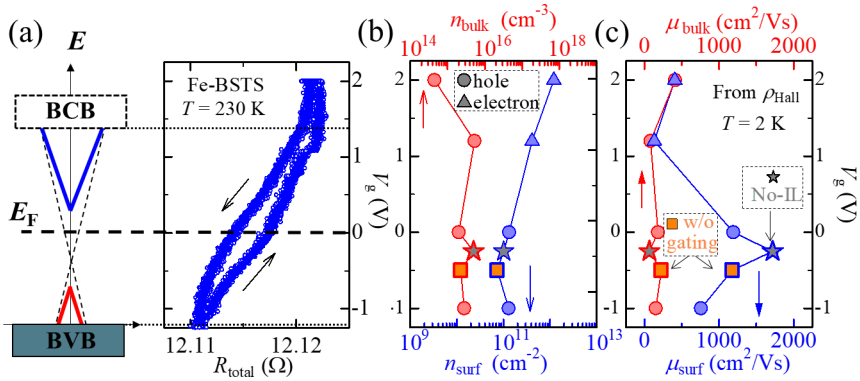

Figure 4. Schematic band structure and analytical results for IL-gated Fe-BSTS. (a) Schematic band structure and transfer characteristics (R_{total} vs V_G) of the EDLT-based Fe-BSTS bulk crystal at 230 K. The dotted lines correspond to the estimated BCB, BVB, and Fermi energy level of bulk bands and V_G. Voltage dependence of (b) carrier and (c) mobility for bulk (red) and surface (blue). The circle and triangle symbols represent the above parameters of holes and electrons, respectively. The star and square symbols are estimated at the V_G position for the No-IL and w/o gating cases, respectively.

coherence length l_ϕ can be evaluated as $B_\phi = \frac{\hbar}{4el_\phi}$. Almost perfect fitting results were obtained in the temperature range of 2−50 K. The power-law fit of the coherence length above 20 K yielded $T^{-0.45} \sim T^{-1/2}$, indicating two-dimensional decay[46,49] (inset of Figure 3d). Interestingly, the coherence length below 10 K deviates from the $T^{-1/2}$ curve and is suppressed at approximately 10 K where most magnetic TIs show a ferromagnetic transition.[22,23] The Hall resistivity showed gentle curves, indicating that at least two components should exist. Here, we applied the standard two-band model (within the Drude model in low-field) fitting to the Hall resistivity, assuming the surface and bulk contributions described in ref 50.

$$\rho_{xy}(B) = \frac{(R_{H,surf}\rho_{bulk}^{\ 2} + R_{H,bulk}\rho_{surf}^{\ 2})B + R_{H,surf}R_{H,bulk}(R_{H,surf} + R_{H,bulk})B^3}{(\rho_{surf} + \rho_{H,bulk})^2 + (R_{H,surf} + R_{H,bulk})^2B^2}$$

where $R_H(\rho)_{surf/bulk}$ represents the Hall coefficients (resistivity) for surface/bulk, respectively. This model is widely applied for TIs.[17,51] Using the standard relation, we can obtain the sample parameters as follows: $R_{H,surf} = \frac{t}{en_{surf}}$, $R_{H,bulk} = \frac{1}{en_{bulk}}$, and $\mu_{surf/bulk} = \frac{R_{H,surf/bulk}}{\rho_{surf/bulk}}$, where t, n_{surf}, and n_{bulk} are the sample thickness and carrier densities of the surface and bulk, respectively. As a result, we obtained an excellent fit (dashed lines in Figure 3b and Figure S3c for the temperature dependence of the No-IL sample). The fitting parameters obtained are summarized in Figure 3d. The temperature dependence of the carrier density and mobility showed typical p-type semiconducting behavior, ensuring the validity of the analytical fitting. The surface mobility exceeded 1500 $cm^2/(V\,s)$, which makes the plot of Hall resistivity curved. EDLT gating mainly tunes these surface states and thus enables us to evaluate the surface states, even using a bulk crystal.

Figure 4a shows the gate-voltage dependence of resistance at 230 K, where the bulk contribution dominates almost the entire transport. Despite a small change in the resistance, a small hysteretic loop appeared. The loop traced the same cyclic loops at least three times even at different sweep speeds (1−2 mV/s). This loop represents only a unipolar nature similar to the bulk MoS_2[44] and $(Bi_{1-x}Sb_x)_2Te_3$ thin film[52] at this temperature. However, low-temperature transport drastically affected the IL-gating effect. Figure 3b shows the Hall resistance at 2 K for different gate voltages. Note that, even just loading the IL onto the sample, the resistance drastically dropped at low temperatures (Figure 3a), and the slope of the Hall resistance decreased, meaning that the IL itself leads to hole doping. All the Hall resistance showed gentle curves like the No-IL case, including V_G = +2 and +1.2 V which look linear. As shown in the inset of Figure 3b, the slope of V_G = +2 V was negative, indicating successful electron doping by the IL gating. MR was also changed by gating (Figure S3d). These facts indicate that the IL gating onto the bulk crystal achieved bipolar transport.

Figure 4a−c shows summarized fitting results from the two-band model. The bulk hole carrier slightly decreased with elevating gate voltage, while the surface carrier showed the p−n carrier-type transition around +0.5 V. The surface mobility drastically dropped to the bulk value when the V_G = +1.2 V and −1 V, indicating that the chemical potential of V_G = 1.2 (−1) V is located near the BCB (BVB). The analyses also revealed that the surface contribution also changed from 26% (No-IL) to 60% (2 V), comparable to previous reports using a thin-film sample[53] and nanowires.[45] Considering the trends of the gated properties, we can estimate the location of the surface chemical potential of No-IL and w/o gating. The appropriate positions are −0.25 V for No-IL and −0.5 V for w/o gating, resulting in smoothly connected carrier density lines. The highest mobility should reflect the nearest chemical potential to the DP, and thus, the Fermi energy of the as-grown crystal (No-IL) is closest to the DP. Therefore, this IL-gated-transport measurement also indicates that the location of the DP is just below the Fermi energy level. To achieve fine E_F tuning just onto the DP using IL gating, the promising gate voltage is approximately 0.25 V, where the p−n carrier-type for the surface carriers changes. These analyses with the two-band model consistently explain all the gated-transport measurements and support the STM/STS conclusion of the ideal E_F

https://doi.org/10.1021/acs.jpclett.1c00869
J. Phys. Chem. Lett. 2021, 12, 4180−4186

and DP positions. Therefore, we conclude that Fe-BSTS is a promising bulk material for observing quantum phenomena driven by the massive Dirac cone at very low temperatures wherein the excitation is well suppressed by the surrounding temperature.

In summary, we investigated the surface band structures of Fe-BSTS via STS/STM and IL-gated-transport measurements. The local STS measurement showed two notable features of the surface state: the DP near the Fermi level and the gapped states at the DP (4 K normalized spectra), implying a magnetic gap opening. The IL-gated-transport measurement combined with the two-band analyses also supports that the DP is near the ideal position. Both results can consistently be understood within the framework of the band structure of Figure 1b,c, ensuring the magnetic gap and the Fermi energy above the DP. Therefore, the Fe-BSTS bulk single crystal is a promising platform for detecting exotic phenomena such as the QAH effect.

METHODS

We grew single crystals of Fe-BSTS using a modified Bridgman method referred to as Fe- or Mn-doped Bi_2Se_3,[36] Fe-doped Bi_2Te_2Se,[28] and Fe-doped $BSbT_2Se$.[29] The details of crystal growth and sample characterization are described in the Supporting Information. STM/STS measurements were performed using JT-SPM (SPECS). The crystals were mechanically cleaved in an ultrahigh vacuum (UHV, $\sim 10^{-10}$ mbar). The transport properties were evaluated using a PPMS (Quantum Design Inc.) with an external gate-voltage source/current monitor R6244 (Advantest). Details of the IL-gating configuration are provided in the Supporting Information.

ASSOCIATED CONTENT

Supporting Information

The Supporting Information is available free of charge at https://pubs.acs.org/doi/10.1021/acs.jpclett.1c00869.

Crystal preparation and characterization, EDLT device fabrication process, and detailed magnetotransport properties of the as-grown crystal (PDF)

AUTHOR INFORMATION

Corresponding Authors

Rikizo Yano − *Institute of Materials and Systems for Sustainability and Applied Physics, Nagoya University, Nagoya 464-8603, Japan;* orcid.org/0000-0003-1959-311X; Email: yano-rikizo@nagoya-u.jp

Vasily S. Stolyarov − *TQPSS Lab, Center for Photonics and 2D Materials, Moscow Institute of Physics and Technology, Dolgoprudny, Moscow Oblast 141700, Russia; Dukhov Research Institute of Automatics (VNIIA), Moscow 127055, Russia;* orcid.org/0000-0002-5317-0818; Email: vasiliy.stoliarov@gmail.com

Satoshi Kashiwaya − *Applied Physics, Nagoya University, Nagoya 464-8603, Japan*; Email: s.kashiwaya@nagoya-u.jp

Authors

Andrei Kudriashov − *TQPSS Lab, Center for Photonics and 2D Materials, Moscow Institute of Physics and Technology, Dolgoprudny, Moscow Oblast 141700, Russia*

Hishiro T. Hirose − *Laboratory for Materials and Structures, Tokyo Institute of Technology, Yokohama 226-8503, Japan;* orcid.org/0000-0001-5912-0881

Taiki Tsuda − *Applied Physics, Nagoya University, Nagoya 464-8603, Japan*

Hiromi Kashiwaya − *National Institute of Advanced Industrial Science and Technology (AIST), Tsukuba 305-8568, Japan*

Takao Sasagawa − *Laboratory for Materials and Structures, Tokyo Institute of Technology, Yokohama 226-8503, Japan*

Alexander A. Golubov − *TQPSS Lab, Center for Photonics and 2D Materials, Moscow Institute of Physics and Technology, Dolgoprudny, Moscow Oblast 141700, Russia; Faculty of Science and Technology and MESA+ Institute of Nanotechnology, Enschede 7500 AE, The Netherlands*

Complete contact information is available at: https://pubs.acs.org/10.1021/acs.jpclett.1c00869

Author Contributions

[+]R.Y. and V.S.S. contributed equally to this work.

Notes

The authors declare no competing financial interest.

ACKNOWLEDGMENTS

The authors thank Prof. Yukio Tanaka and Dr. Kohei Tsumura for fruitful discussions. This study was supported by JST CREST (Grant No. JPMJCR16F2) and KAKENHI (Grant Nos. JP15H05851, 15H05853, 16H03847, 18H01243, 20H00131, 21H04652, and 21K13854), Researcher Exchange Program between JSPS and RFBR (JPJSBP120194816), and JSPS Core-to-Core program "Oxide Superspin" (OSS) international network (Grant JPJSCCA20170002). Crystal growth was supported by Collaborative Research Projects in MSL-Tokyo Tech., Japan. A.A.G. and V.S.S. acknowledge the Grant RSF-ANR 20-42-09033.

REFERENCES

(1) Hasan, M. Z.; Kane, C. L. *Colloquium*: Topological Insulators. *Rev. Mod. Phys.* **2010**, *82*, 3045−3067.

(2) Qi, X.-L.; Zhang, S.-C. Topological Insulators and Superconductors. *Rev. Mod. Phys.* **2011**, *83*, 1057−1110.

(3) Kou, L.; Ma, Y.; Sun, Z.; Heine, T.; Chen, C. Two Dimensional Topological Insulators: Progress and Prospects. *J. Phys. Chem. Lett.* **2017**, *8*, 1905−1919.

(4) Ando, Y. Topological Insulator Materials. *J. Phys. Soc. Jpn.* **2013**, *82*, 102001.

(5) Si, N.; Yao, Q.; Jiang, Y.; Li, H.; Zhou, D.; Ji, Q.; Huang, H.; Li, H.; Niu, T. Recent Advances in Tin: From Two-Dimensional Quantum Spin Hall Insulator to Bulk Dirac Semimetal. *J. Phys. Chem. Lett.* **2020**, *11*, 1317−1329.

(6) Kane, C. L.; Mele, E. J. Z_2 Topological Order and the Quantum Spin Hall Effect. *Phys. Rev. Lett.* **2005**, *95*, 146802.

(7) Xue, H.; Lv, W.; Wu, D.; Cai, J.; Ji, Z.; Zhang, Y.; Zeng, Z.; Jin, Q.; Zhang, Z. Temperature Dependence of Spin−Orbit Torques in Nearly Compensated $Tb_{21}Co_{79}$ Films by a Topological Insulator Sb_2Te_3. *J. Phys. Chem. Lett.* **2021**, *12*, 2394−2399.

(8) Fu, L.; Kane, C. L.; Mele, E. J. Topological Insulators in Three Dimensions. *Phys. Rev. Lett.* **2007**, *98*, 106803.

(9) Pi, S.-T.; Wang, H.; Kim, J.; Wu, R.; Wang, Y.; Lu, C.-K. New Class of 3D Topological Insulator in Double Perovskite. *J. Phys. Chem. Lett.* **2017**, *8*, 332−339.

(10) Tian, L.; Liu, Y.; Meng, W.; Zhang, X.; Dai, X.; Liu, G. Spin-Orbit Coupling-Determined Topological Phase: Topological Insulator and Quadratic Dirac Semimetals. *J. Phys. Chem. Lett.* **2020**, *11*, 10340−10347.

(11) Qi, X.-L.; Hughes, T. L.; Zhang, S.-C. Topological Field Theory of Time-Reversal Invariant Insulators. *Phys. Rev. B* **2008**, *78*, 195424.

(12) Majorana, E.; Maiani, L. *Ettore Majorana Scientific Papers*; Springer, 2006; pp 201−233.
(13) Burset, P.; Lu, B.; Tkachov, G.; Tanaka, Y.; Hankiewicz, E. M.; Trauzettel, B. Superconducting Proximity Effect in Three-Dimensional Topological Insulators in the Presence of a Magnetic Field. *Phys. Rev. B* **2015**, *92*, 205424.
(14) Kushwaha, S.; Pletikosić, I.; Liang, T.; Gyenis, A.; Lapidus, S.; Tian, Y.; Zhao, H.; Burch, K.; Lin, J.; Wang, W.; et al. Sn-Doped $Bi_{1.1}Sb_{0.9}Te_2S$ Bulk Crystal Topological Insulator with Excellent Properties. *Nat. Commun.* **2016**, *7*, 11456.
(15) Ren, Z.; Taskin, A.; Sasaki, S.; Segawa, K.; Ando, Y. Optimizing $Bi_{2-x}Sb_xTe_{3-y}Se_y$ Solid Solutions to Approach the Intrinsic Topological Insulator Regime. *Phys. Rev. B* **2011**, *84*, 165311.
(16) Pan, Y.; Wu, D.; Angevaare, J. R.; Luigjes, H.; Frantzeskakis, E.; Jong, N. d.; Heumen, E. v.; Bay, T. V.; Zwartsenberg, B.; Huang, Y. K.; et al. Low Carrier Concentration Crystals of the Topological Insulator $Bi_{2-x}Sb_xTe_{3-y}Se_y$: a Magnetotransport Study. *New J. Phys.* **2014**, *16*, 123035.
(17) Ren, Z.; Taskin, A.; Sasaki, S.; Segawa, K.; Ando, Y. Large Bulk Resistivity and Surface Quantum Oscillations in the Topological Insulator Bi_2Te_2Se. *Phys. Rev. B* **2010**, *82*, 241306.
(18) Stolyarov, V. S.; Yakovlev, D. S.; Kozlov, S. N.; Skryabina, O. V.; Lvov, D. S.; Gumarov, A. I.; Emelyanova, O. V.; Dzhumaev, P. S.; Shchetinin, I. V.; Hovhannisyan, R. A.; et al. Josephson Current Mediated by Ballistic Topological States in $Bi_2Te_{2.3}Se_{0.7}$ Single Nanocrystals. *Commun. Mater.* **2020**, *1*, 38.
(19) Chang, C.-Z.; Zhang, J.; Feng, X.; Shen, J.; Zhang, Z.; Guo, M.; Li, K.; Ou, Y.; Wei, P.; Wang, L.-L.; et al. Experimental Observation of the Quantum Anomalous Hall Effect in a Magnetic Topological Insulator. *Science* **2013**, *340*, 167−170.
(20) Chang, C.-Z.; Tang, P.; Wang, Y.-L.; Feng, X.; Li, K.; Zhang, Z.; Wang, Y.; Wang, L.-L.; Chen, X.; Liu, C.; et al. Chemical-Potential-Dependent Gap Opening at the Dirac Surface States of Bi_2Se_3 Induced by Aggregated Substitutional Cr Atoms. *Phys. Rev. Lett.* **2014**, *112*, 056801.
(21) Liu, W.; West, D.; He, L.; Xu, Y.; Liu, J.; Wang, K.; Wang, Y.; van der Laan, G.; Zhang, R.; Zhang, S.; et al. Atomic-Scale Magnetism of Cr-Doped Bi_2Se_3 Thin Film Topological Insulators. *ACS Nano* **2015**, *9*, 10237−10243.
(22) Collins-McIntyre, L. J.; Harrison, S. E.; Schönherr, P.; Steinke, N.-J.; Kinane, C. J.; Charlton, T. R.; Alba-Veneroa, D.; Pushp, A.; Kellock, A. J.; Parkin, S. S. P.; et al. Magnetic Ordering in Cr-Doped Bi_2Se_3 Thin Films. *EPL* **2014**, *107*, 57009.
(23) Baker, A.; Figueroa, A.; Kummer, K.; Collins-McIntyre, L. J.; Hesjedal, T.; van der Laan, G. Magnetic Proximity-Enhanced Curie Temperature of Cr-Doped Bi_2Se_3 Thin Films. *Phys. Rev. B* **2015**, *92*, 094420.
(24) Deng, Y.; Yu, Y.; Shi, M. Z.; Guo, Z.; Xu, Z.; Wang, J.; Chen, X. H.; Zhang, Y. Quantum Anomalous Hall Effect in Intrinsic Magnetic TopologicalInsulator $MnBi_2Te_4$. *Science* **2020**, *367*, 895−900.
(25) Ji, H.; Allred, J. M.; Ni, N.; Tao, J.; Neupane, M.; Wray, A.; Xu, S.; Hasan, M. Z.; Cava, R. J. Bulk Intergrowth of a Topological Insulator with a Room-Temperature Ferromagnet. *Phys. Rev. B* **2012**, *85*, 165313.
(26) Stolyarov, V. S.; Remizov, S. V.; Shapiro, D. S.; Pons, S.; Vlaic, S.; Aubin, H.; Baranov, D. S.; Brun, C.; Yashina, L. V.; Bozhko, S. I.; et al. Double Fe-Impurity Charge State in the Topological Insulator Bi_2Se_3. *Appl. Phys. Lett.* **2017**, *111*, 251601.
(27) Desvignes, L.; Stolyarov, V. S.; Aprili, M.; Massee, F. Tunable High Speed Atomic Rotor in Bi_2Se_3 Revealed by Current Noise. *ACS Nano* **2021**, *15*, 1421−1425.
(28) Yano, R.; Koyanagi, M.; Kashiwaya, H.; Tsumura, K.; Hirose, H. T.; Asano, Y.; Sasagawa, T.; Kashiwaya, S. Unusual Superconducting Proximity Effect in Magnetically Doped Topological Josephson Junctions. *J. Phys. Soc. Jpn.* **2020**, *89*, 034702.
(29) Yano, R.; Hirose, H. T.; Tsumura, K.; Yamamoto, S.; Koyanagi, M.; Kanou, M.; Kashiwaya, H.; Sasagawa, T.; Kashiwaya, S. Proximity-Induced Superconducting States of Magnetically Doped 3D Topological Insulators with High Bulk Insulation. *Condens. Matter* **2019**, *4*, 9.
(30) Ko, W.; Park, J.; Jeon, I.; Kim, H. W.; Kwon, H.; Oh, Y.; Kim, J. S.; Suh, H.; Hwang, S. W.; Chung, C. Local Potential Fluctuation of Topological Surface States in $Bi_{1.5}Sb_{0.5}Te_{1.7}Se_{1.3}$ Observed by Landau Level Spectroscopy. *Appl. Phys. Lett.* **2016**, *108*, 083109.
(31) Ko, W.; Jeon, I.; Kim, H. W.; Kwon, H.; Kahng, S.-J.; Park, J.; Kim, J. S.; Hwang, S. W.; Suh, H. Atomic and Electronic Structure of an Alloyed Topological Insulator, $Bi_{1.5}Sb_{0.5}Te_{1.7}Se_{1.3}$. *Sci. Rep.* **2013**, *3*, 2656.
(32) Stolyarov, V. S.; Sheina, V. A.; Khokhlov, D. A.; Vlaic, S.; Pons, S.; Aubin, H.; Akzyanov, R. S.; Vasenko, A. S.; Menshchikova, T. V.; Chulkov, E. V.; et al. Disorder-Promoted Splitting in Quasiparticle Interference at Nesting Vectors. *J. Phys. Chem. Lett.* **2021**, *12*, 3127−3134.
(33) Netsou, A.-M.; Muzychenko, D. A.; Dausy, H.; Chen, T.; Song, F.; Schouteden, K.; Van Bael, M. J.; Van Haesendonck, C. Identifying Native Point Defects in the Topological Insulator Bi_2Te_3. *ACS Nano* **2020**, *14*, 13172−13179.
(34) Hanaguri, T.; Igarashi, K.; Kawamura, M.; Takagi, H.; Sasagawa, T. Momentum-Resolved Landau-level Spectroscopy of Dirac Surface State in Bi_2Se_3. *Phys. Rev. B* **2010**, *82*, 081305.
(35) Stolyarov, V. S.; Pervakov, K. S.; Astrakhantseva, A. S.; Golovchanskiy, I. A.; Vyalikh, D. V.; Kim, T. K.; Eremeev, S. V.; Vlasenko, V. A.; Pudalov, V. M.; Golubov, A. A.; et al. Electronic Structures and Surface Reconstructions in Magnetic Superconductor $RbEuFe_4As_4$. *J. Phys. Chem. Lett.* **2020**, *11*, 9393−9399.
(36) Chen, Y.; Chu, J.-H.; Analytis, J.; Liu, Z.; Igarashi, K.; Kuo, H.-H.; Qi, X.; Mo, S.-K.; Moore, R.; Lu, D.; et al. Massive Dirac Fermion on the Surface of a Magnetically Doped Topological Insulator. *Science* **2010**, *329*, 659−662.
(37) Wray, L. A.; Xu, S.-Y.; Xia, Y.; Hsieh, D.; Fedorov, A. V.; San Hor, Y.; Cava, R. J.; Bansil, A.; Lin, H.; Hasan, M. Z. A Topological Insulator Surface under Strong Coulomb, Magnetic and Disorder Perturbations. *Nat. Phys.* **2011**, *7*, 32−37.
(38) Xu, S.-Y.; Neupane, M.; Liu, C.; Zhang, D.; Richardella, A.; Wray, L. A.; Alidoust, N.; Leandersson, M.; Balasubramanian, T.; Sánchez-Barriga, J.; et al. Hedgehog Spin Texture and Berry's Phase Tuning in a Magnetic Topological Insulator. *Nat. Phys.* **2012**, *8*, 616−622.
(39) Tsukahara, N.; Shiraki, S.; Itou, S.; Ohta, N.; Takagi, N.; Kawai, M. Evolution of Kondo Resonance From a Single Impurity Molecule to the Two-Dimensional Lattice. *Phys. Rev. Lett.* **2011**, *106*, 187201.
(40) Misra, R.; McCarthy, M.; Hebard, A. F. Electric Field Gating with Ionic Liquids. *Appl. Phys. Lett.* **2007**, *90*, 052905.
(41) Ueno, K.; Nakamura, S.; Shimotani, H.; Ohtomo, A.; Kimura, N.; Nojima, T.; Aoki, H.; Iwasa, Y.; Kawasaki, M. Electric-Field-Induced Superconductivity in an Insulator. *Nat. Mater.* **2008**, *7*, 855−858.
(42) Saito, Y.; Nojima, T.; Iwasa, Y. Gate−Induced Superconductivity in Two-Dimensional Atomic Crystals. *Supercond. Sci. Technol.* **2016**, *29*, 093001.
(43) Ye, J.; Zhang, Y. J.; Akashi, R.; Bahramy, M. S.; Arita, R.; Iwasa, Y. Superconducting Dome in a Gate-Tuned Band Insulator. *Science* **2012**, *338*, 1193−1196.
(44) Zhang, Y.; Ye, J.; Matsuhashi, Y.; Iwasa, Y. Ambipolar MoS_2 Thin Flake Transistors. *Nano Lett.* **2012**, *12*, 1136−1140.
(45) Hsiung, T.-C.; Mou, C.-Y.; Lee, T.-K.; Chen, Y.-Y. Surface-Dominated Transport and Enhanced Thermoelectric Figure of Merit in Topological Insulator $Bi_{1.5}Sb_{0.5}Te_{1.7}Se_{1.3}$. *Nanoscale* **2015**, *7*, 518−523.
(46) Bao, L.; He, L.; Meyer, N.; Kou, X.; Zhang, P.; Chen, Z.-g.; Fedorov, A. V.; Zou, J.; Riedemann, T. M.; Lograsso, T. A.; et al. Weak Anti-Localization and Quantum Oscillations of Surface States in Topological Insulator Bi_2Se_2Te. *Sci. Rep.* **2012**, *2*, 726.
(47) Jia, S.; Ji, H.; Climent-Pascual, E.; Fuccillo, M.; Charles, M.; Xiong, J.; Ong, N. P.; Cava, R. J. Low-Carrier-Concentration Crystals of the Topological Insulator Bi_2Te_2Se. *Phys. Rev. B* **2011**, *84*, 235206.

https://doi.org/10.1021/acs.jpclett.1c00869
J. Phys. Chem. Lett. 2021, 12, 4180−4186

(48) Hikami, S.; Larkin, A. I.; Nagaoka, Y. Spin-Orbit Interaction and Magnetoresistance in the Two Dimensional Random System. *Prog. Theor. Phys.* **1980**, *63*, 707−710.
(49) Altshuler, B. L.; Aronov, A.; Khmelnitsky, D. Effects of Electron-Electron Collisions with Small Energy Transfers on Quantum Localisation. *J. Phys. C: Solid State Phys.* **1982**, *15*, 7367−7386.
(50) Ashcroft, N. W.; Mermin, N. D. *Solid State Physics*; Harcourt, Inc.: Orlando, FL; 1976; p 240.
(51) Xia, B.; Ren, P.; Sulaev, A.; Liu, P.; Shen, S.-Q.; Wang, L. Indications of Surface-Dominated Transport in Single Crystalline Nanoflake Devices of Topological Insulator $Bi_{1.5}Sb_{0.5}Te_{1.8}Se_{1.2}$. *Phys. Rev. B* **2013**, *87*, 085442.
(52) Shimizu, S.; Yoshimi, R.; Hatano, T.; Takahashi, K. S.; Tsukazaki, A.; Kawasaki, M.; Iwasa, Y.; Tokura, Y. Gate Control of Surface Transport in MBE-Grown Topological Insulator $(Bi_{1-x}Sb_x)_2Te_3$ Thin Films. *Phys. Rev. B* **2012**, *86*, 045319.
(53) Hsiung, T.-C.; Chen, D.-Y.; Zhao, L.; Lin, Y.-H.; Mou, C.-Y.; Lee, T.-K.; Wu, M.-K.; Chen, Y.-Y. Enhanced Surface Mobility and Quantum Oscillations in Topological Insulator $Bi_{1.5}Sb_{0.5}Te_{1.7}Se_{1.3}$ Nanoflakes. *Appl. Phys. Lett.* **2013**, *103*, 163111.

https://doi.org/10.1021/acs.jpclett.1c00869
J. Phys. Chem. Lett. 2021, 12, 4180−4186